Proceedings of the
Annual Stability Conference
Structural Stability Research Council
Atlanta, Georgia, April 21-24, 2026

Strength and stability assessment of cold-formed steel storage rack stub columns after exposure to elevated temperatures

Pandiri Nithish Reddy[1],. Jashnav Pancheti[2]

Abstract

Cold-formed steel (CFS) sections are used in the manufacturing of storage racks due to their high strength-to-weight ratio and ease of manufacturing. The overall stability of the storage racks is primarily governed by the uprights (columns). When these CFS upright members are exposed to fire, it has a significant impact on the load-carrying capacity and overall stability of the storage rack. As steel regains most of its strength post the fire exposure, structural elements can be reused if the structure has not collapsed during the fire. This paper investigates the residual mechanical properties of steel and the load-carrying capacity of CFS stub columns after exposure to elevated temperatures. The tensile coupons were cut from hot-rolled, pickled, and oiled steel sheet of grade E250, with thicknesses of 1.6 and 2.5 mm. The specimens were heated to a predetermined elevated temperature of 300–900 °C. From the experimental results, it was found that the mechanical properties and load-carrying capacity of the stub column were reduced when compared to the specimens that were not exposed to elevated temperature. Using these experimental results finite element model was developed and validated. This study also compares the current DSM-based design approach with the experimental data and numerical data for calculating the residual post-fire strength of the CFS storage rack upright.

1. Introduction

Cold-formed steel (CFS) has become one of the most favorable materials for construction in the industry (Karabulut & Soyoz, 2017) due to its cost efficiency, high strength and easy fabrication in various cross sections and sizes. Due to their high slenderness and open cross-section, these members may experience local, distortional, and global buckling, or any potential interaction among these buckling modes of failure, depending on the cross-section geometry, boundary conditions, and loading scenarios, which can lead to geometric failure prior to material failure. The post-buckling reserve strength for local buckling is greater, but it is negligible for distortional and global buckling failure types. The local buckling and post-buckling reserve strength can be improved through the addition of stiffeners in the cross-sections.

[1] Doctoral Research Scholar, Indian Institute of Technology Tirupati, India, <ce24d004@iittp.ac.in>
[2] Assistant Professor, Indian Institute of Technology Tirupati, India, <Jashnav@iittp.ac.in>

In the storage industry, these CFS sections are used as uprights, beams and bracings. These uprights contain an array of perforations along the length of flanges and web, which allows beams and bracings to be connected at variable heights. Due to these perforations, the design of the upright is complicated. Despite several studies examining the impact of perforations on the strength of structural elements, a conclusive analytical solution for storage rack members remains unidentified. Consequently, the current design standards recommend a design-by-testing approach to determine the load-bearing capacity of storage rack members. Recently, numerous studies have investigated the applicability of the Direct Strength Method (DSM), a widely used design approach for thin-walled structures. These studies highlighted the limitations of the conventional DSM when applied to perforated members and proposed modified formulations to explicitly account for the effects of perforations in strength prediction.

In the event of a fire accident, the temperature in the surroundings will increase rapidly. When these CFS members are exposed to such elevated temperatures, their load-carrying capacity will decrease rapidly, leading to early collapse. Structural fire safety is an essential component that must be taken into consideration in the design stage. In contrast, there are no standard guidelines for the fire design of these structures. After the occurrence of fire, the temperature eventually starts reaching room temperature, during this cooling phase, the residual forces and deformations will make the situation much more severe (Fang & Chan, 2022). At room temperature, CFS exhibits good mechanical properties, but when the temperature rises, steel loses its strength and stiffness (Fang & Chan, 2022). But most steel buildings exposed to fire can still be reused because steel has a higher residual strength after cooling from high temperatures. According to Kirby (Smith et al., 1981), steel members that have been damaged by fire can be categorized into three groups: Members that have been slightly damaged by a fire and have either no or very slight deformations are classified as Category 1; these can be reused directly. Members that have deformations and which can be made straight are classified as Category 2; these can be used if the straightening process is cost effective. Members that have substantial deformations are classified as Category 3; these must typically be replaced with new sections. But to reuse them after fire incidents it is important to determine the residual material properties and the maximum temperature it is exposed to.

The residual mechanical properties of various types of steel after exposure to elevated temperatures were evaluated by. (Chen et al., 2021; Gunalan & Mahendran, 2014; Kesawan & Mahendran, 2018; Qiang et al., 2012; Ren et al., 2020; Yan et al., 2021) and observed various factors that affect the mechanical properties. The studied nominal yield stress ranges from 235 MPa to 1200 MPa with a thickness range of 0.75 to 5 mm. In comparison with low-strength steel, the high-strength steel experiences relatively high loss in the residual strength when compared to its initial strength with no exposure to elevated temperatures (Gunalan & Mahendran, 2014). The cooling regimes, mainly cooled in air (CIA) and cooled in water (CIW) have a significant influence on the residual mechanical properties (Ren et al., 2020). The studies (Chen et al., 2021; Kesawan & Mahendran, 2018) highlights the difference in reduction factors between tensile coupons made from sections and sheets.(Pons et al., 2022; Ye & Ozaki, 2021; Zuo et al., 2024) studied the member stability of cold-formed steel columns after exposure to elevated temperatures with various cross-sections. (Pons et al., 2022; Ye & Ozaki, 2021) studied the post-fire buckling strength of CFS square hollow sections with thicknesses of 1.6 mm and 3.2 mm. (Zuo et al., 2024) conducted experimental studies on the post-elevated temperature behaviour of CFS elliptical hollow stub columns; the temperature

curve adopted in the study was the standard fire curve (ISO-834 fire curve). Most studies have focused on the post-fire material properties of CFS members; however, the stability of CFS columns after exposure to elevated temperatures has not been extensively studied.

This study focuses on the assessment of the strength and stability of CFS storage rack stub columns after exposure to elevated temperatures. It involves the experimental investigation of the residual mechanical properties of E250, 1.6 mm and 2.5 mm thick, after exposure to elevated temperatures. The residual compression capacities of CFS storage rack stub columns were evaluated using both experimental and numerical studies. In the experimental study, the stub columns were exposed to four different temperatures and cooled naturally to room temperature. The finite element model was used to build and validate the residual compression capacities of the stub column after exposure to elevated temperatures, and a detailed parametric study was done. This study also compares the current DSM-based design approach with experimental data and numerical data for calculating the residual post-fire strength of the CFS storage rack upright.

2. Experimental Studies

2.1 Tensile Coupon tests

Tensile coupon tests are performed on E250 grade steel, 1.6 mm and 2.5 mm thick. The specimens were cut from HRPO steel sheets, and the dimensions are mentioned in Fig. 1. The specimen's length was 250 mm, with a width of 12mm and a gauge length of 50 mm. The specimen surface does not contain any coatings of paint or zinc and are cleaned before heating. Initial dimensions were taken with a help digital vernier calliper with the least count of 0.001 mm. Using an electric furnace, the test specimens were heated to predefined elevated temperatures, 300 °C, 400 °C, 500 °C, 600 °C, 700 °C, 800 °C and 900 °C as shown in Fig. 2, the test specimens are heated to the target temperature at a rate of 10 °C/min (Mushahary et al., 2021). After the temperature reaches the target temperature, it was kept constant for 20 minutes to have a uniform distribution of temperature (Pons et al., 2022). The specimens were cooled in the furnace without the use of artificial cooling or quenching techniques. The samples were removed after the furnace temperature reached room temperature. Emery paper was used to clean the specimens to remove any scales that had formed on the surface and final measurements were taken.

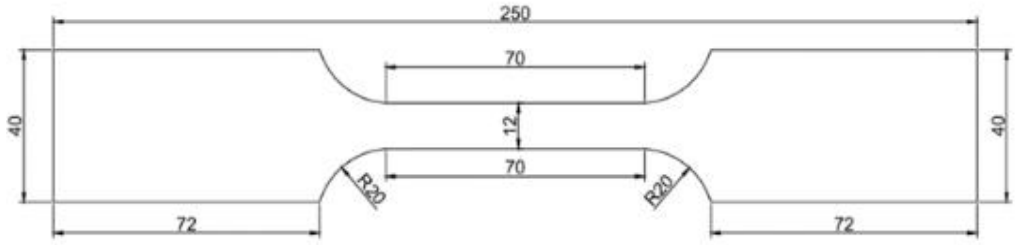

Figure 1: Tensile Coupon

The tensile coupon specimen was placed in an MTS testing apparatus of 100 kN capacity, as seen in Fig. 3**.** The specimen was placed between the grips of the testing machine. In the loading test setup, the top grip was free to move, whereas the bottom end was held in place. The tests followed

the guidelines of (ASTM E8) and are displacement-controlled, with a loading rate of 0.005 mm/sec until the yield point is reached and at a loading rate of 0.4 mm/min until fracture (Huang & Young, 2014).

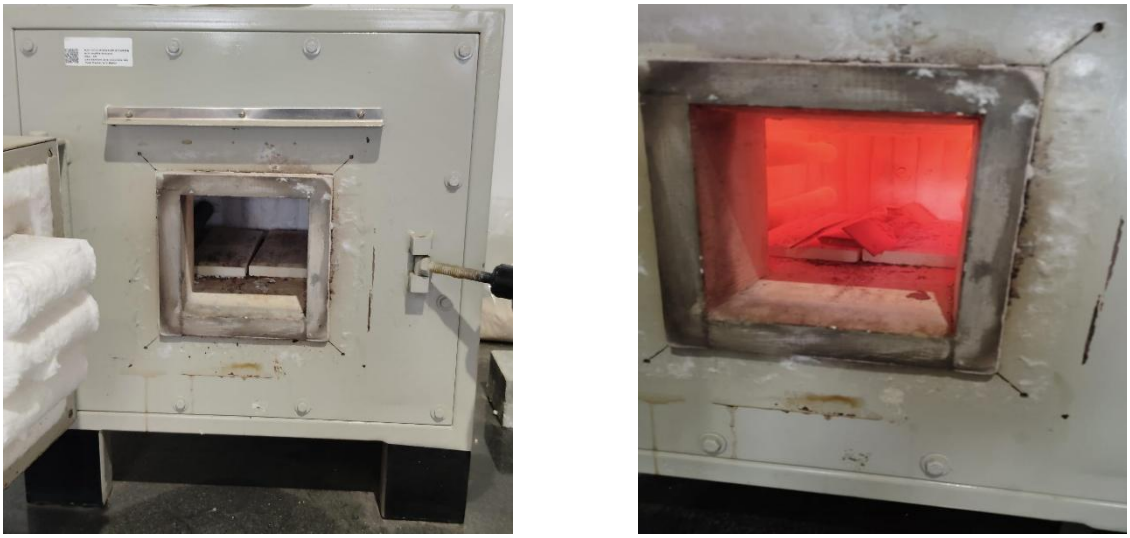

Figure 2: Electric furnace for heating

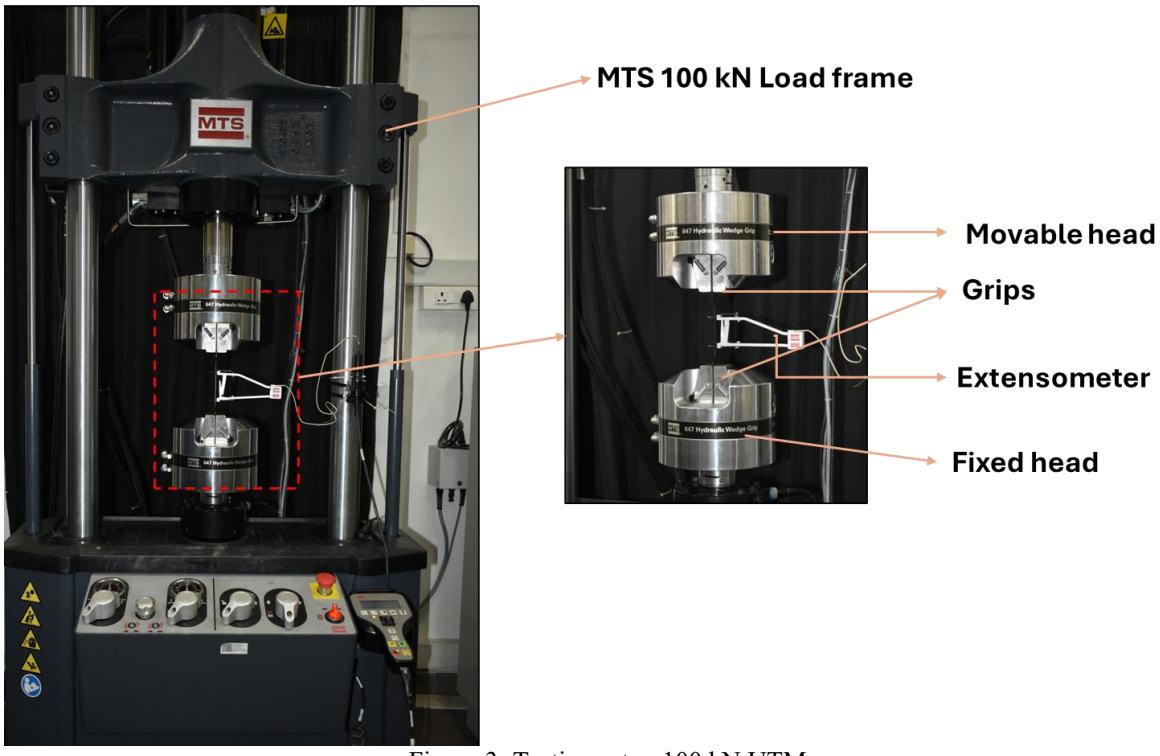

Figure 3: Testing setup 100 kN UTM

Stress-strain experimental results are presented in Fig. 4, with the temperature to which each sample was exposed indicated in the legend. These curves demonstrate a significant difference

between test specimens subjected to no exposure to elevated temperatures and those tested after exposure to elevated temperatures. Tables 1 and 2 present the average residual mechanical properties, including yield strength, ultimate strength, and elastic modulus, along with the corresponding residual reduction factors.

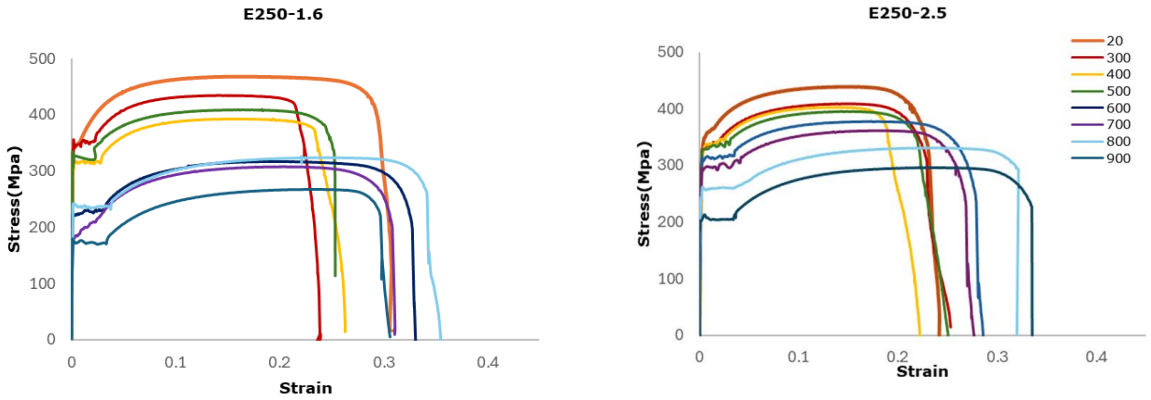

Figure 4: Stress-strain curves

Table 1: Residual mechanical properties and reduction factors for E250 grade 1.6 mm thick

Specimen ID	E_T(Gpa)	$\sigma_{y,T}$ (Mpa)	$\sigma_{u,T}$ (Mpa)	E_T/E_{20}	$\sigma_{y,T}/\sigma_{0.2,20}$	$\sigma_{u,T}/\sigma_{u,20}$
E 250-1.6-20	229.0	343.0	468.0	1.0	1.0	1.0
E 250-1.6-300	225.00	334.0	435.0	1.0	1.0	0.9
E 250-1.6-400	221.00	317.0	412.0	1.0	0.9	0.9
E 250-1.6-500	223.00	310.0	394.0	1.0	0.9	0.8
E 250-1.6-600	225.00	302.0	385.0	1.0	0.9	0.8
E 250-1.6-700	220.00	247.0	371.0	1.0	0.7	0.8
E 250-1.6-800	221.00	240.0	326.0	1.0	0.7	0.7
E 250-1.6-900	216.00	172.0	267.0	0.9	0.5	0.6

Table 2: Residual mechanical properties and reduction factors for E250 grade 2.5 mm thick

Specimen ID	E_T(Gpa)	$\sigma_{y,T}$ (Mpa)	$\sigma_{u,T}$ (Mpa)	E_T/E_{20}	$\sigma_{y,T}/\sigma_{0.2,20}$	$\sigma_{u,T}/\sigma_{u,20}$
E 250-2.5-20	219.7	349.1	429.2	1.0	1.0	1.0
E 250-2.5-300	227.4	333.7	408.9	1.0	1.0	1.0
E 250-2.5-400	224.6	323.5	402.6	1.0	0.9	0.9
E 250-2.5-500	221.3	328.9	395.7	1.0	0.9	0.9
E 250-2.5-600	221.1	306.7	378.3	1.0	0.9	0.9
E 250-2.5-700	217.4	291.1	361.4	1.0	0.8	0.8
E 250-2.5-800	207.7	238.3	330.3	0.9	0.7	0.8
E 250-2.5-900	209.6	193.4	296.1	1.0	0.6	0.7

Generally, increasing the exposure temperature resulted in a reduction in strength for all specimens. The residual reduction factors are calculated as the ratio of the mechanical property (elastic modulus, yield strength and ultimate strength) of the specimen tested after exposure to the elevated temperature to the specimen with no exposure to elevated temperature. The elastic modulus was evaluated using the stress–strain slope between 10% and 50% of the yield stress, as per ISO 6892-1:2016. For E250 steel of 1.6 mm and 2.5 mm thickness, no significant reduction in residual elastic modulus was observed up to 800 °C, while a slight decrease of less than 10% occurred at 900 °C. The residual yield strength of E250 steel (1.6 mm) decreased progressively with increasing temperature, retaining approximately 90% up to 600 °C and reducing to about 50% at 900 °C. A similar trend was observed for the 2.5 mm thick specimens, which maintained over

90% at 600 °C and about 60% at 900 °C. The residual ultimate strength of 1.6 mm thick E250 steel remained around 90% up to 400 °C and reduced to about 60% at 900 °C, whereas the 2.5 mm thick specimens retained approximately 90% at 600 °C and around 70% at 900 °C.

2.2 Stub-column tests

The tests were performed to study the residual compression capacities of E250-grade, 1.6 mm-thick CFS storage rack stub-columns after exposure to elevated temperatures. A total of 10 stub columns were tested, of which 2 were tested at ambient conditions without any elevated temperature exposure, and the remaining were tested after exposure to high temperatures of 300 °C, 500 °C, 700 °C and 900 °C. The heating and cooling procedure followed is the same as that of the tensile coupon test process. The cross-sectional shape and typical perforation locations and dimensions at the web and flange are shown in Fig. 5**.** The length of the specimens was chosen to be three times the greater cross-sectional dimension to account for the effect of residual stresses and geometrical imperfections (EN 15512). The illustration shows that there are quadrilateral and circular perforations at the web and flanges, respectively. These perforations extend along the length of the upright, enabling the beam to be connected at different heights, as well as for connecting steel bracings.

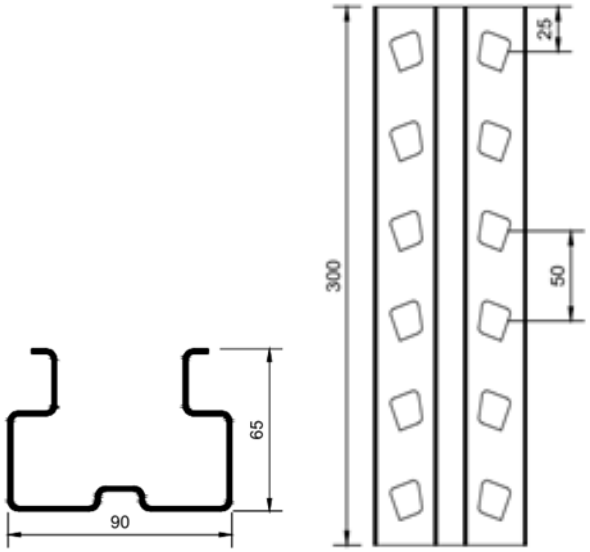

Figure 5: Cross-section dimensions

The stub column specimens were placed on a 250 kN capacity Zwick Roell compression testing machine. The top and bottom of each specimen were welded with endplates measuring 110 mm by 85 mm. The welded stub columns were placed between the top crosshead and the lower actuator. The test was conducted using a displacement-controlled method with a loading rate of 0.05 mm/min (Huang & Young, 2014) and a preload of 4 kN was applied. Four linear variable differential transformers (LVDTs) were used to measure the axial shortening and transverse deflection of flanges and web. The arrangement of these LVDTs is shown in Fig. 6. The axial shortening was measured by one vertical LVDT, and the transverse displacement of the web and both left and right flanges was measured by three horizontal LVDTs. These LVDT readings were recorded with the help of the HBM Data Acquisition System. The residual compression test set-up is shown in Fig. 7.

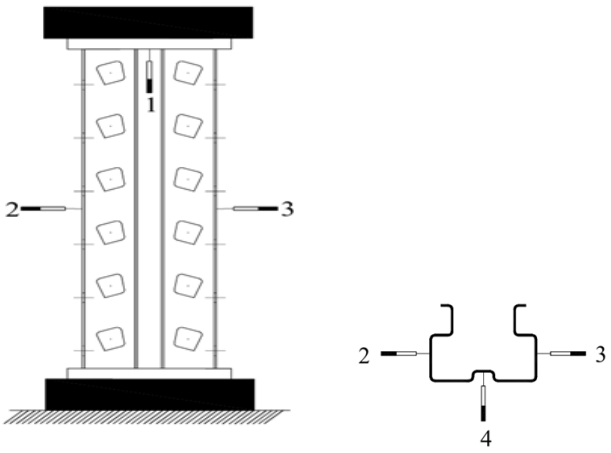

Figure 6: LVDT arrangement

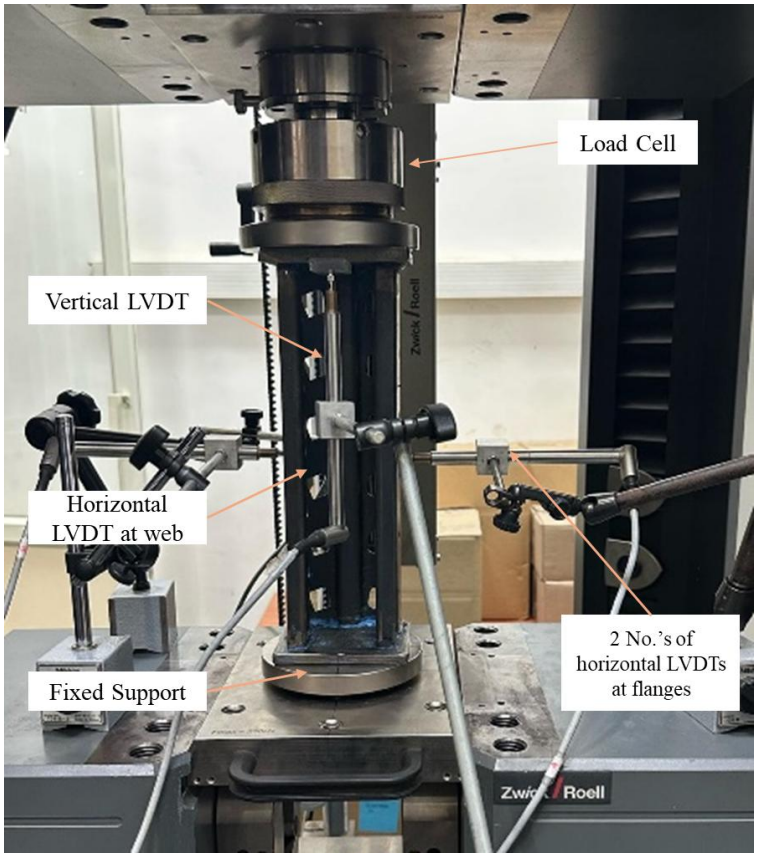

Figure 7: Compression testing test set-up

The compressive strengths of axially loaded stub columns, determined through experimental testing, are summarized in Table 3. Additionally, the load-displacement behaviour of stub columns subjected to elevated temperatures was analysed and compared with that of columns not exposed to elevated temperatures. All the specimens were observed to fail by distortional buckling. A buckling failure of a typical section is shown in Fig. 8.

Table 3: Residual ultimate load capacities

Specimen	Specimen-1	Specimen-2	Average Ultimate load (P_{ul}) kN
E250-1.6--20	125.65	115.36	120.5
E250-1.6--300	118.28	123	120.6
E250-1.6--500	114.22	103.37	108.87
E250-1.6--700	94.51	*	94.51
E250-1.6--900	59.48	49	54.24

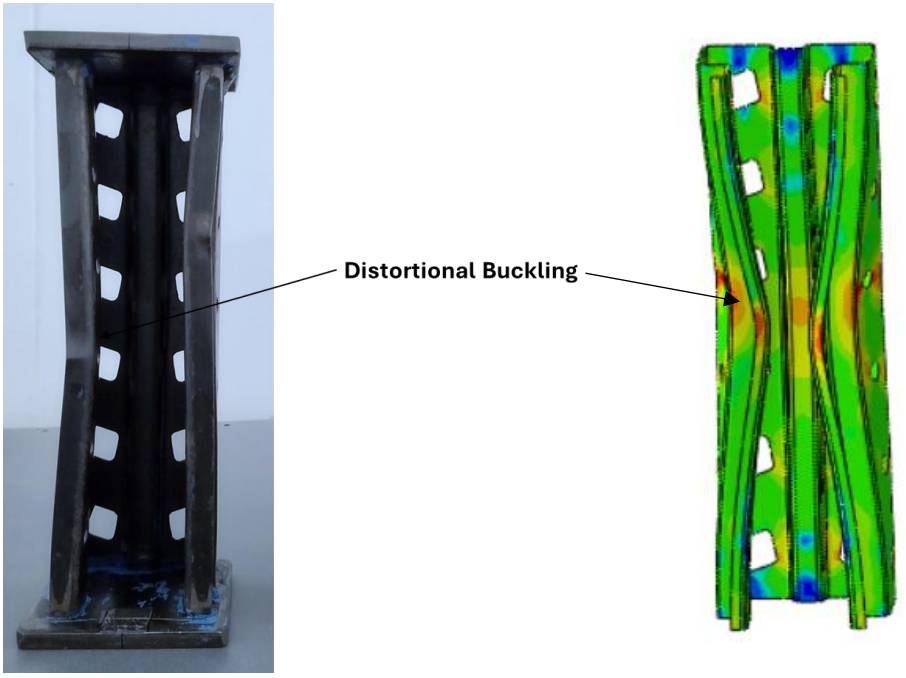

Experiment failure mode FE failure mode

Figure 8: Comparison of experiment and FE

3. Numerical study.

3.1 Development of numerical model

To resemble the compression behaviour of the stub columns at ambient and post-elevated temperature exposure, a nonlinear finite element model was simulated in Abaqus software. The dimensions incorporated in the model are shown in Fig. 5. The type of element selected was four nodded shell with reduced integration (S4R). Linear elastic buckling analysis is performed initially. The values for modulus of elasticity and yield stress are taken from the experimental results reported in Table 1. For the non-linear analysis, the engineering stress-strain values obtained from the experiments are changed into true stress and strain values. The true stress, along with plastic strain, is used for non-linear analysis (Singh & Singh, 2021)

To account for the initial local geometric imperfection, the lowest elastic buckling mode shape was determined using eigenvalue analysis and then amplified to produce the necessary imperfection profile along the specimen length. The imperfection amplification factor was chosen based on the numerical models of members not been exposed to fire. The non-linear analysis is

carried out using the Static Riks method to capture the experimental behaviour essentially. The mesh size for the model adopted was 2 × 2 mm² (Shabhari et al., 2024). The meshing is done finer around the perforations of the stub columns to obtain a smooth transition from the perforation area to the non-perforated area which is depicted in Fig. 9. A reference point passing through the centroid of the omega shaped cross section is created to which MPC beam constraint is imposed Fig. 10. To mimic the fixed support given in experiment, only axial displacement at the loading point is allowed, while all other translational and rotational degrees of freedom are restrained.

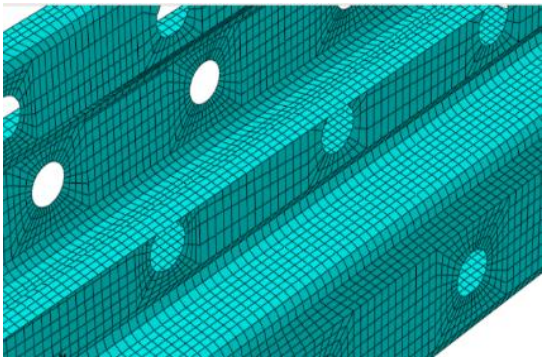

Figure 9: FE Model meshing

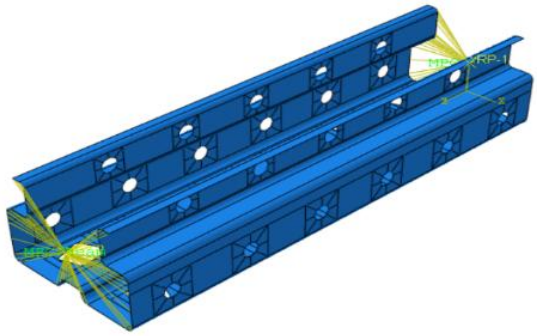

Figure 10: MPC Beam constraint

3.2 Numerical model results

The numerical model validation results in terms of residual compression strength of CFS storage rack stub columns after exposure to elevated temperature are tabulated in Table 4. The mean and coefficient of variation (COV) values of P_{Exp}/P_{FE} are 0.92 and 1.65, respectively, where P_{Exp} is the experimental compressive strength, and P_{FE} is the numerical compressive strength. Additionally, load–axial shortening curves acquired from the experiments and FE analyses are compared. Fig 11 shows the comparison results of load vs axial deformation curves between FE and experimental results of CFS storage rack stub columns after exposure to elevated temperature. The results indicated that the developed FE model for stub columns exhibited the ability to accurately replicate the key experimental results in terms of residual compressive strength and load-displacement response. The typical failure mode of the numerical model and comparison with the experimental mode of failure is shown in Fig. 8.

Table 4: Comparison of FE and experimental test results

Specimen	($P_{ul.\ Exp}$) kN	($P_{ul.\ FE}$)	$P_{ul.\ FE}$ / $P_{ul.\ Exp}$
E250-1.6-20	120.5	112.05	0.93
E250-1.6-300	120.6	109.8	0.91
E250-1.6-500	108.87	96.15	0.88
E250-1.6-700	94.51	79.41	0.84
E250-1.6-900	54.24	53.80	0.98
		Mean	0.92
		Coefficient of variation	1.65

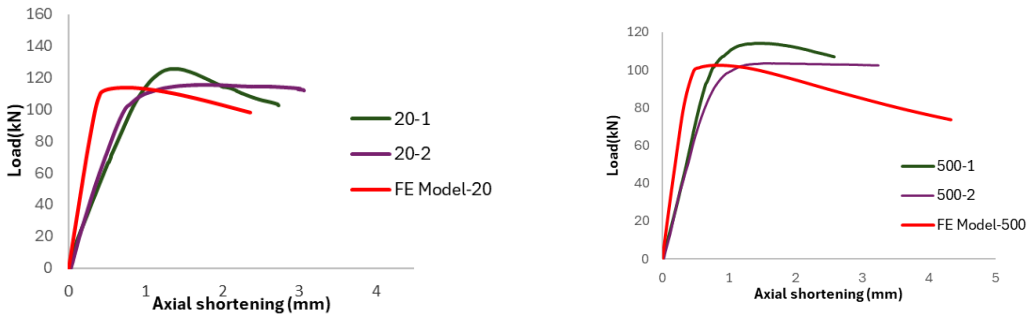

Figure 11: Comparison between experiment and FE analysis

4. Design strength predictions

To evaluate the applicability of current design methodologies for predicting the residual storage rack upright resistance after exposure to elevated temperatures, obtained from this study were compared with the design strengths derived using the Direct Strength Method (DSM) according to AISI S 100-20024 The DSM equations for the calculation of nominal global, distortional, and local for the perforated members are as per clause E2 (GB), E4 (DB) and E3.2(LB), respectively, from AISI S 100-20024 for perforated members are outlined below:

Global Buckling (P_{ne})

$$P_{ne} = A_g F_n \quad (1)$$

$$F_n = 0.658^{\lambda_c^2} \times F_y \quad \text{if } \lambda_c \leq 1.5 \quad (2)$$

$$F_n = \left(\frac{0.877}{\lambda_c^2}\right) \times F_y \quad \text{if } \lambda_c > 1.5 \quad (3)$$

$$\lambda_c = \sqrt{\frac{F_y}{F_{cre}}}$$

Local Buckling (P_{nl})

$$P_{nl} = 1.2(P_{y,net})\left(\frac{1 + 0.1\lambda_l^{\,2}}{1 + 0.55\lambda_l^{\,2}\left(\frac{P_{y,net}}{P_{ne}}\right)}\right) \quad (4)$$

$$\lambda_l = \sqrt{\frac{P_{ne}}{P_{crl}}}$$

Distortional Buckling (P_{nd})

$$P_{nd} = 1.2(P_{y,net})\left(\frac{1 + 0.05\lambda_d^{\,2}}{1 + 0.67\lambda_d^{\,2}\left(\frac{P_{y,net}}{P_{ne}}\right)}\right) \quad (5)$$

$$\lambda_l = \sqrt{\frac{P_y}{P_{crd}}}$$

Where, Ag is gross cross-section area, Anet is net cross-section area, F_y is yield stress, P_{ne} is Nominal global buckling capacity, P_{cre} is Critical elastic global buckling capacity, P_{nl} is Nominal local buckling capacity, P_{crl} is Critical elastic local buckling capacity, P_{nd} is Nominal distortional

buckling capacity P_{crd} is Critical elastic distortional buckling capacity P_y - Yield load ($A_g \times F_y$), $P_{y,net}$ is Yield load corresponding to net area ($A_{net} \times F_y$). The elastic buckling capacities are determined by finite element analysis by selecting the appropriate buckling mode shape. The elastic buckling mode shapes and corresponding buckling modes are shown in Fig. 12. The residual compression capacities of the storage rack stub-columns obtained from the experiment and FE analysis DSM are presented in Table 5. According to the DSM design specifications, the compression capacity of the member must be sufficient to withstand local, Distortional, and Global buckling loads, i.e., a minimum of three buckling loads.

Table 5: Comparison of DSM predictions with experimental and FE load capacities

Specimen ID	$P_{ul.\ Exp}$ (kN)	$P_{ul.\ FE}$ (kN)	DSM load (P_{DSM})	$P_{DSM}/P_{ul.\ Exp}$
E250-1.6-20	120.5	112.05	117.18	0.97
E250-1.6-300	120.6	109.8	114.11	0.95
E250-1.6-400	-	97.34	108.31	-
E250-1.6-500	108.87	96.15	105.91	0.97
E250-1.6-600	-	93.13	103.18	-
E250-1.6-700	94.51	79.42	83.39	0.88
E250-1.6-800	-	73.64	82.00	-
E250-1.6-900	54.24	53.80	58.76	1.08

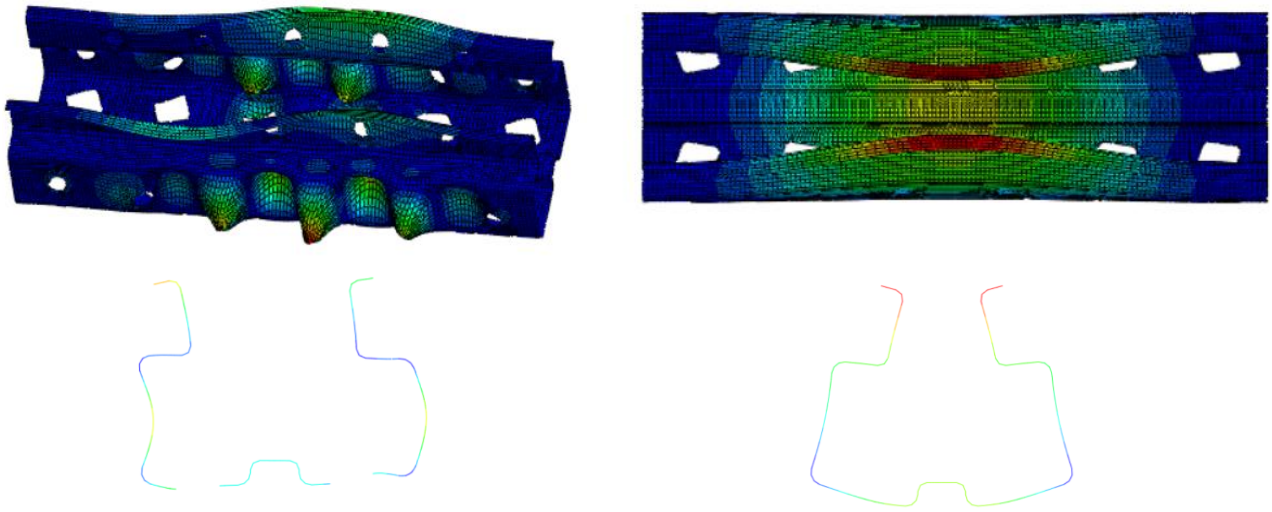

Local buckling mode Distortional buckling mode

Figure 12: Elastic buckling modes for DSM

For the 300 mm length stub column, elastic buckling analysis indicated that only local and distortional buckling modes were present, and the minimum eigenvalue corresponding to these modes was adopted for DSM predictions. For all specimens, the distortional buckling load was lower than the local buckling load and hence governed the DSM strength calculations. Overall, DSM captures the trend in residual compression strength well, but consistently underestimates. Compared with experimental results, the DSM-to-experimental strength ratios were generally in the range of approximately 0.88–1.0, indicating conservative predictions. In contrast, compared with the FE results, the residual compression capacities predicted by DSM are close to the experimental results.

5. Conclusions

The residual compression behavior of CFS storage rack uprights after exposure to elevated temperatures was studied through experimental investigations, numerical studies and design strength predictions using DSM. The experimental investigation involved tensile coupon tests to study the residual mechanical properties of E250 grade steel with thicknesses of 1.6 mm and 2.5 mm, exposed to a temperature range of 300 °C to 900 °C. Additionally, 10 CFS storage rack stub uprights were exposed to temperatures of 300 °C, 500 °C, 700 °C, and 900 °C and residual compression capacities were calculated. Some conclusions drawn from the present study are summarised as follows:

- The residual mechanical tests indicated that the elastic modulus remained relatively constant after exposure to 900 °C; however, both yield strength and ultimate strength exhibited a significant decrease in their reduction factors when subjected to temperatures exceeding 600 °C, thereby affecting the overall residual strength.
- The residual compression tests on CFS storage stub columns after exposure to elevated temperature showed a gradual decrease in compressive strength with an increase in temperature, and observed distortional buckling mode as the primary failure mode of stub columns.
- The Nonlinear finite element models were developed and compared with experimental data, with an average FE-to-experimental ultimate load ratio of 0.92, indicating that the numerical model slightly underestimates the experimental capacity.
- The experimental results and numerical results were also compared with the DSM design strength predictions. The DSM strength predictions exhibited comparatively better correlation with experimental results, with most DSM-to-experimental ratios close to one. When compared to the FE results, DSM always predicts slightly larger ultimate loads. This shows that it continuously overestimates compared to numerical predictions.
- A detailed parametric analysis is to be conducted to propose suitable modifications to the existing design equations for enhanced strength prediction after exposure to elevated temperatures. Furthermore, experiments on actual-size CFS storage rack upright specimens after the heating and cooling processes are required in future work.

References

Chen, M. T., Pandey, M., & Young, B. (2021). Post-fire residual material properties of cold-formed steel elliptical hollow sections. Journal of Constructional Steel Research, 183. https://doi.org/10.1016/j.jcsr.2021.106723

EN15512:2009. Steel static storage systems–adjustable pallet racking systems–principles for structural design. CEN:Brussels; 2009.

Fang, H., & Chan, T. M. (2022). Behaviour and design of cold-formed normal- and high-strength steel SHS and RHS columns at elevated temperatures. Thin-Walled Structures, 180. https://doi.org/10.1016/j.tws.2022.109947

Gunalan, S., & Mahendran, M. (2014). Experimental investigation of post-fire mechanical properties of cold-formed steels. Thin-Walled Structures, 84, 241–254. https://doi.org/10.1016/j.tws.2014.06.010

Huang, Y., & Young, B. (2014). The art of coupon tests. Journal of Constructional Steel Research, 96, 159–175. https://doi.org/10.1016/j.jcsr.2014.01.010

Karabulut, B., & Soyoz, S. (2017). Experimental and analytical studies on different configurations of cold-formed steel structures. Journal of Constructional Steel Research, 133, 535–546. https://doi.org/10.1016/j.jcsr.2017.02.027

Kesawan, S., & Mahendran, M. (2018). Post-fire mechanical properties of cold-formed steel hollow sections. Construction and Building Materials, 161, 26–36. https://doi.org/10.1016/j.conbuildmat.2017.11.077

Mushahary, S. K., Singh, K. D., & Jayachandran, S. A. (2021). Mechanical properties of E350 steel during heating and cooling. Thin-Walled Structures, 160. https://doi.org/10.1016/j.tws.2020.107351

Pons, D., Lapuebla-Ferri, A., & Romero, M. L. (2022). Post-fire Residual Strength and Ductility of Structural Steels from Hollow Sections https://doi.org/10.1002/cepa.1777

Qiang, X., Bijlaard, F. S. K., & Kolstein, H. (2012). Post-fire mechanical properties of high strength structural steels S460 and S690. Engineering Structures, 35, 1–10. https://doi.org/10.1016/j.engstruct.2011.11.005

Ren, C., Dai, L., Huang, Y., & He, W. (2020). Experimental investigation of post-fire mechanical properties of Q235 cold-formed steel. Thin-Walled Structures, 150. https://doi.org/10.1016/j.tws.2020.106651

Shabhari, A., Jeyapragasam, V. V. K., & Chandrasekar, D. (2024). Local buckling behaviour of web perforated cold-formed steel lipped channel columns. Thin-Walled Structures, 205, 112448. https://doi.org/10.1016/J.TWS.2024.112448

Singh, T. G., & Singh, K. D. (2021). Design of perforated cold-formed steel hollow stub columns using direct strength method. Thin-Walled Structures, 168, 108265. https://doi.org/10.1016/J.TWS.2021.108265

Smith, C. I., Kirby, B. R., Lapwood, D. G., Cole, K. J., Cunningham, A. P., & Preston, R. R. (1981). The reinstatement of fire damaged steel framed structures. Fire Safety Journal, 4(1), 21–62. https://doi.org/10.1016/0379-7112(81)90004-7

Test Methods for Elevated Temperature Tension Tests of Metallic Materials. (2020). ASTM International. https://doi.org/10.1520/E0021-20

Test Methods for Tension Testing of Metallic Materials. (2022). ASTM International. https://doi.org/10.1520/E0008_E0008M-22

Yan, X., Xia, Y., Blum, H. B., & Gernay, T. (2021). Post-fire mechanical properties of advanced high-strength cold-formed steel alloys. Thin-Walled Structures, 159. https://doi.org/10.1016/j.tws.2020.107293

Ye, K., & Ozaki, F. (2021a). Post-fire mechanical properties and buckling strength of cold-formed steel hollow section columns. Journal of Constructional Steel Research, 184. https://doi.org/10.1016/j.jcsr.2021.106806

Zuo, W., Chen, M. T., & Young, B. (2024a). Structural behaviour of cold-formed steel elliptical hollow section stub columns after exposure to ISO-834 fire curve. Thin-Walled Structures, 197. https://doi.org/10.1016/j.tws.2023.111309

Zuo, W., Chen, M.-T., & Young, B. (2024c). Post-Fire Behavior of Cold-Formed Steel Semi-Oval Hollow Stub Columns. Journal of Structural Engineering, 150(10). https://doi.org/10.1061/jsendh.steng-13392